Supplementary Information

SAMPLES, STANDARDS AND LOCATION

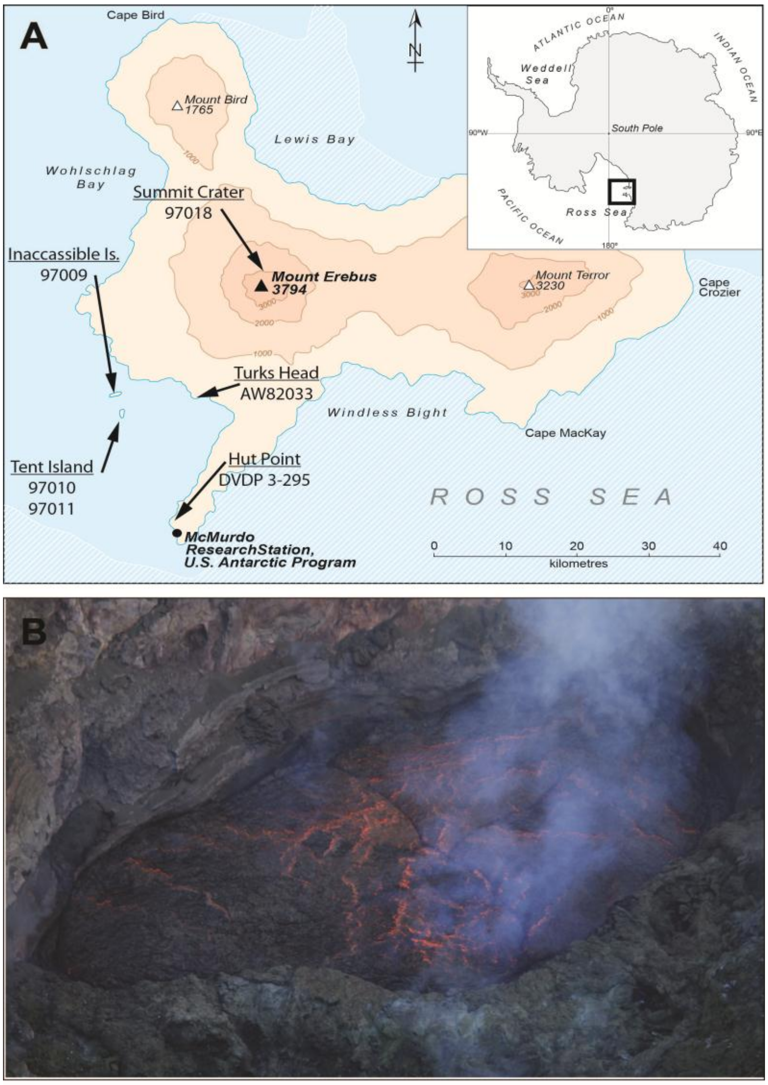

Figure S1*: **A**. Sample location **B**. View of Mt Erebus phonolitic lava lake*

Table S1. Sample sites and lithology (from Eschenbacher, 1998; Oppenheimer *et al.*, 2011)

Sample	Location	Whole rock composition	Occurrence	Remarks
DVDP 3-295	Hut Point	Basanite	Drill core/ hyaloclastite	Drill core sample from the Dry Valley Drilling Project (Kyle and Treves, 1974). This sample from DVDP 3 drill core taken on Hut Point Peninsula at depth of 295 m. Olivine and pyroxene phyric, black basanite pillow breccia..
AW82033	Turks Head	Basanite	Palagonite breccia	Mostly disintegrated sand and gravel sized plagioclase-phyric palagonite breccia with angular glassy lava fragments throughout.
97009	Inaccessible Island	Tephriphonolite	Palagonite breccia	Tephriphonolite palagonite breccia sample from SE Inaccessible Island. The deposit is mostly yellow, sand-sized, bedded palagonite breccia with rare scoriaceous lapilli scattered throughout the unit.
97010	Tent Island	Tephriphonolite	Pillow breccia	Black, plagioclase (minor) phyric, pillow lava breccias from the SE side of Tent Island.
97011	Tent Island	Phonolite	Pillow breccia	As above but from SW side of island and likely stratigraphically higher than 97010.
97018	Near Erebus crater	Phonolite	Lava bomb	Erupted on 21 December 1997.

Table S2. Acquisition parameters at the Fe and S K-edge

Scan Region	Step(eV)	Time(s)
Fe K-edge		
6987-7087	6.25	0.5
7087-7099.5	1.25	2
7099.5-7124.5	0.25	3
7124.5-7200	1.25	0.5
7200-7350	3	0.5
S K-edge		
2400-2460	5	0.5
2460-2500	0.5	1
2500-2560	1	0.5
2560-2675	2	0.5

Table S3. X-ray fluorescence bulk rock analyses of synthetic standards in wt%

Standard	Basanite	Tephriphonolite
SiO_2	42.27	55.28
TiO_2	4.15	1.16
Al_2O_3	13.51	19.38
$Fe_2O_3^T$	13.45	5.67
MnO	0.19	0.20
MgO	8.61	1.21
CaO	10.85	3.09
Na_2O	3.52	7.95
K_2O	1.73	4.04
P_2O_5	0.81	0.47
Loss on ignition	-0.51	0.66
Totals	98.58	99.10

Table S4. EMP analyses of synthetic standards in wt% and associated error.

Sample	SiO2	TiO2	Al2O3	FeO	MgO	CaO	Na2O	K2O	Total
XANSTD_Ba_01_QFM-1	47.99	4.87	14.96	2.67	10.22	12.48	3.63	1.86	98.69
XANSTD_Ba_02_QFM	46.78	4.82	14.69	6.25	10.07	11.74	3.11	1.67	99.12
XANSTD_Ba_03_NNO	44.10	4.57	13.85	10.14	9.76	11.13	3.54	1.74	98.82
XANSTD_Ba_04_NNO+1	42.55	4.45	13.37	13.22	9.26	10.72	3.45	1.68	98.70
XANSTD_TP_01_QFM-1	58.27	1.29	20.46	2.45	1.40	3.28	7.96	4.36	99.47
XANSTD_TP_03_NNO	57.02	1.15	20.18	4.06	1.45	3.31	7.61	4.30	99.22
XANSTD_TP_04_NNO+1	56.07	1.27	19.64	5.88	1.44	3.26	7.52	4.18	99.27
Stdev n = 15									
XANSTD_Ba_01_QFM-1	0.38	0.09	0.16	0.13	0.14	0.17	0.06	0.06	0.57
XANSTD_Ba_02_QFM	0.32	0.10	0.12	0.16	0.12	0.15	0.09	0.07	0.34
XANSTD_Ba_03_NNO	0.36	0.07	0.12	0.27	0.12	0.15	0.08	0.07	0.59
XANSTD_Ba_04_NNO+1	0.33	0.14	0.13	0.26	0.10	0.11	0.09	0.06	0.49
XANSTD_TP_01_QFM-1	0.47	0.04	0.16	0.13	0.09	0.13	0.12	0.12	0.50
XANSTD_TP_03_NNO	0.51	0.05	0.12	0.12	0.06	0.10	0.11	0.13	0.62
XANSTD_TP_04_NNO+1	0.37	0.06	0.10	0.21	0.04	0.11	0.46	0.11	0.56

XANES ANALYTICAL METHODS

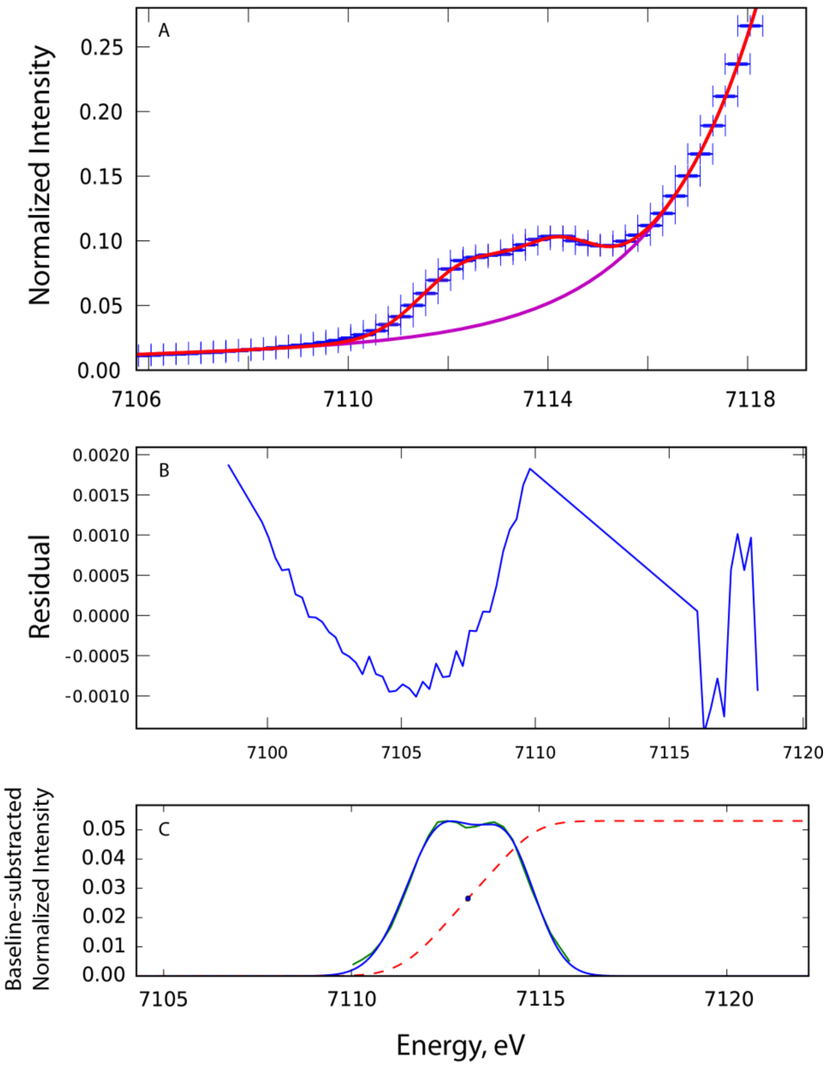

***Figure S2: A**. Pre-edge region fitting. Data point are shown in blue with ±0.25eV error bar. Purple lines shows the baseline absorption of the main Fe absorption edge (linear +DHO functions). The red line shows the entire fitting (linear + DHO + 2 Gaussian functions). **B**. Residual misfit as a function of energy. **C**. The green line represents the baseline-subtracted spectrum, the blue line represents the two Gaussians found to reproduce the spectrum best. The red dotted line represents the cumulative area and the blue dot represents the location of the centroid. The quality of the fit of this sample is representative of all fits in this study.*

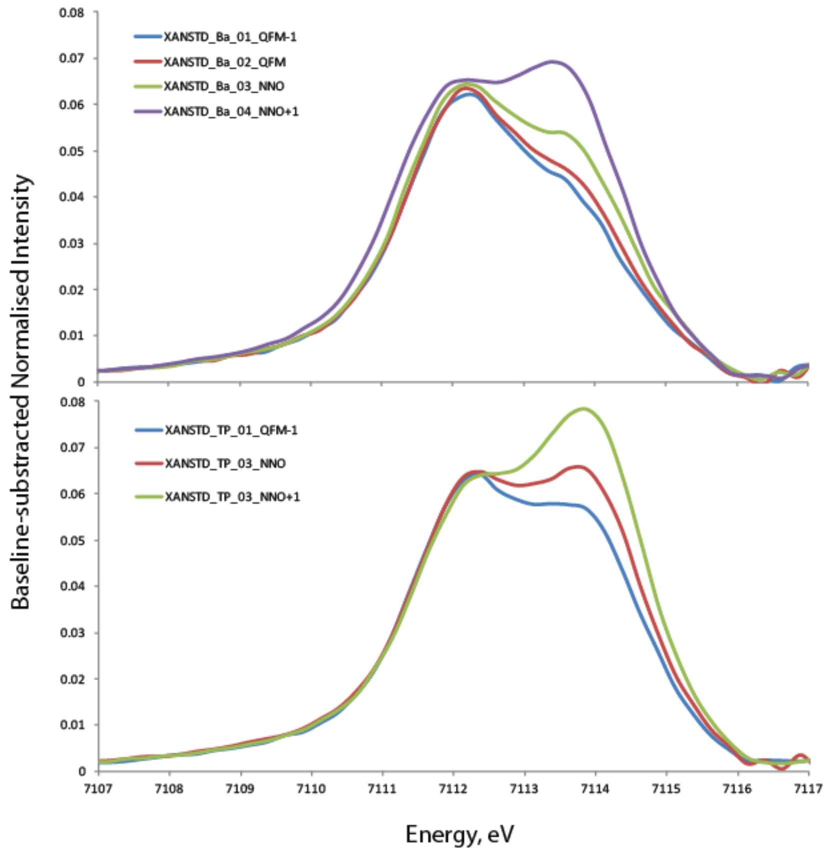

Figure S3: *Background-subtracted (linear +DHO functions) spectra for basanite (upper) and tephriphonolite (lower) standard glasses.*

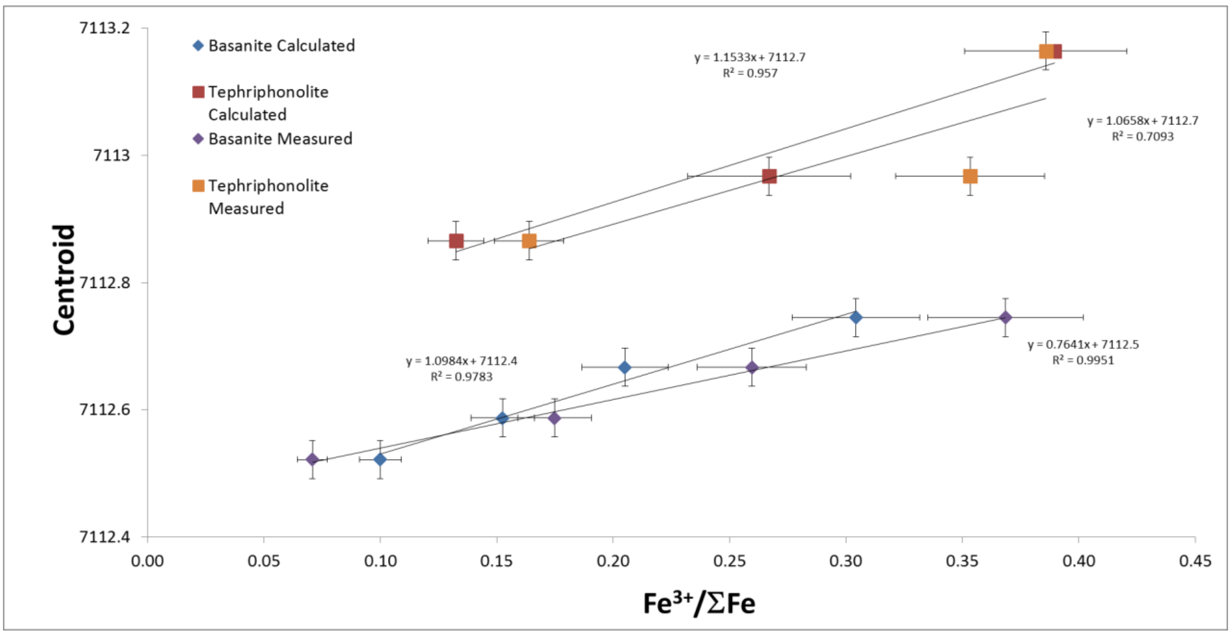

Figure S4: *Same as figure S4 but comparing the standards $Fe^{3+}/\sum Fe$ values of calculated* (see method) *and measured (from wet chemistry) and the resulting effect on the centroid calibration curve.*

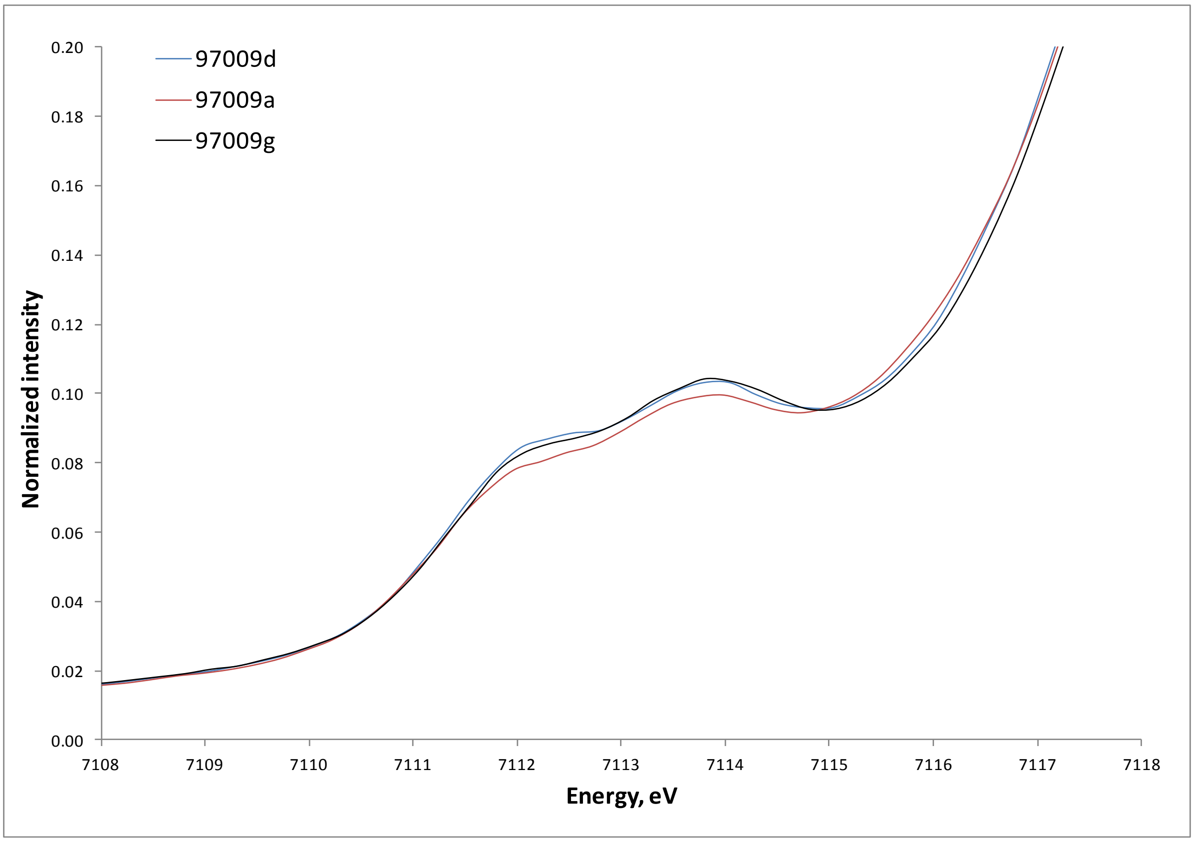

Figure S5: *Example of pre-edge region of three spectra after alignment correcting instrumental energy drift.*

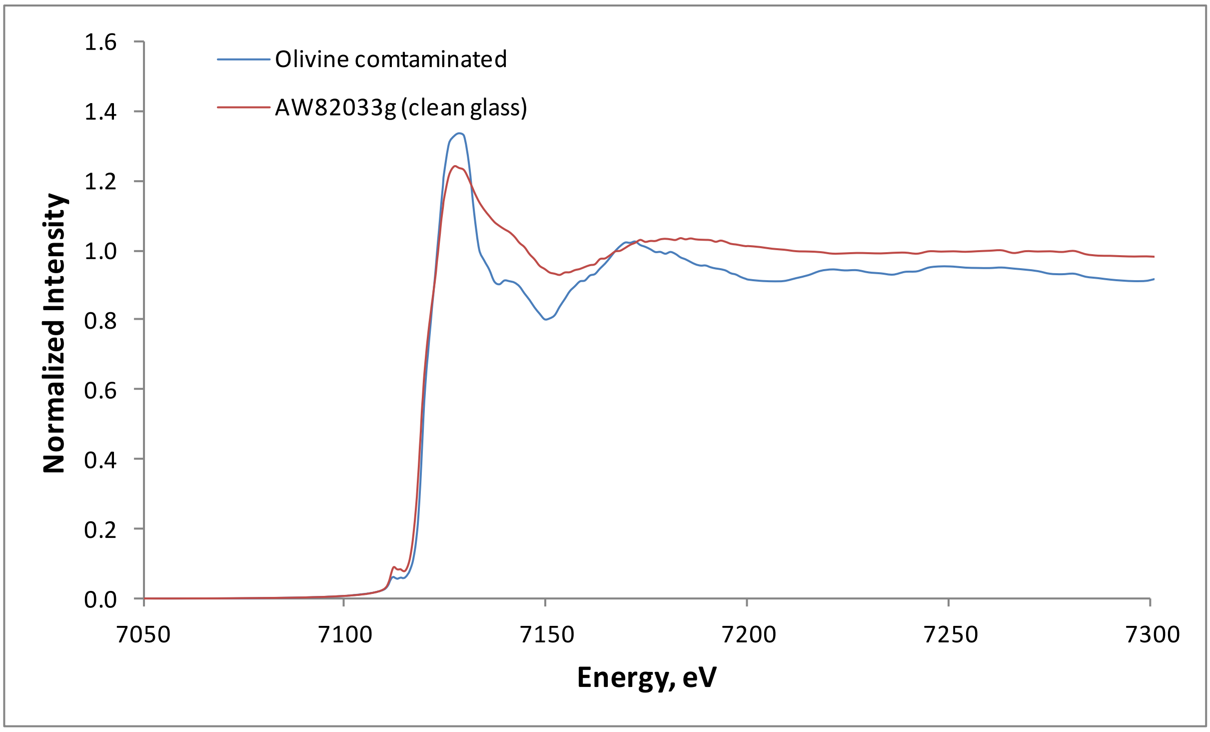

Figure S6: *Example of Fe K-edge spectra of a melt inclusion glass with and without contamination from the olivine host.*

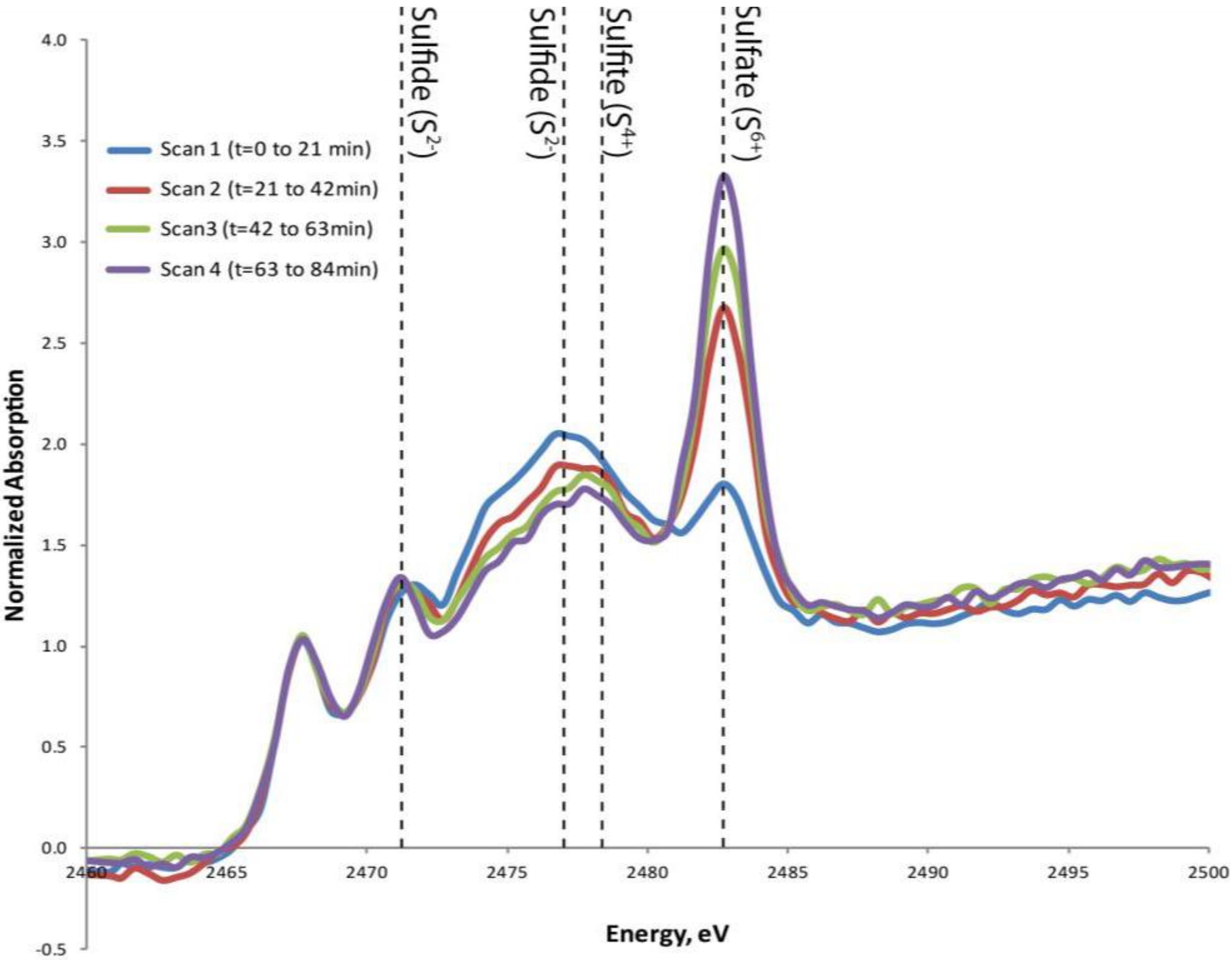

Figure S7: *Time evolution of the sulphur K-edge spectra at a single analysis point from an anorthoclase-hosted melt inclusion showing the progressive oxidation of the sulphur under the beam.*

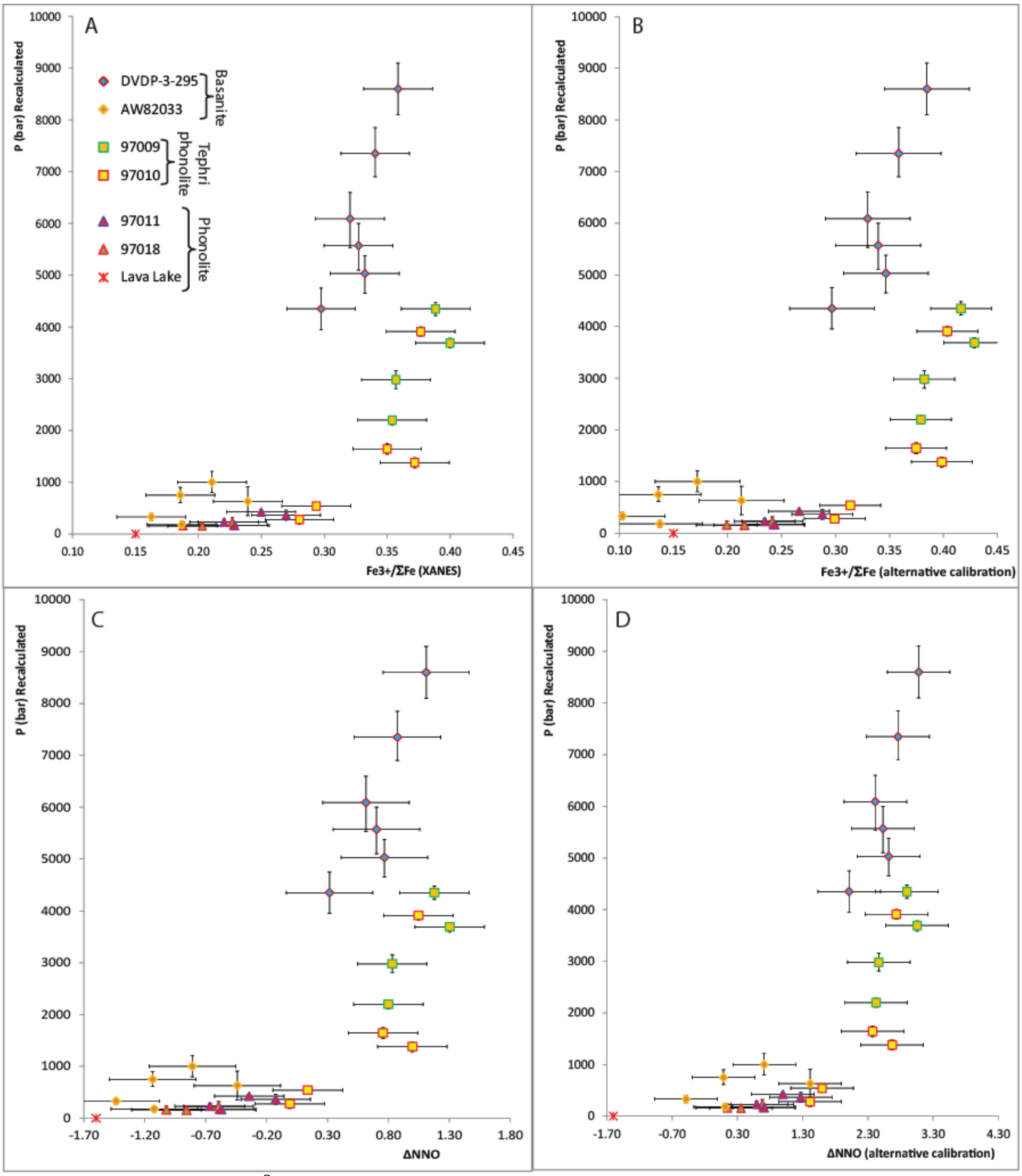

Figure S8: ***A***. *Plot of $Fe^{3+}/\Sigma Fe$ ratios determined by calibrating the centroid position using calculated standard's $Fe^{3+}/\Sigma Fe$ values.* ***B***. *Plot of $Fe^{3+}/\Sigma Fe$ ratios determined by calibrating the centroid position using the measured (wet chemistry) standard's $Fe^{3+}/\Sigma Fe$ values.* ***C***. *Plot of the ΔNNO determined by calibrating the centroid position using the standard's ΔNNO values (as imposed by controlled CO_2/CO gas flux in furnace).* ***D***. *Plot of the ΔNNO determined by calibrating the centroid position using the measured (wet chemistry) standard's ΔNNO values.All data are plotted against the calculated entrapment pressures (this study) for each melt inclusion.*

Table S5. Melt inclusion compositions, all data from Eschenbacher, 1998; Oppenheimer *et al.*, (2011).

	DVDP-3-295											AW82033								
Inclusion	**b**	**c**	**g**	**j**	**q**	**r**	**Mean**	**1σ**	**G1**	**G2**	**G3**	**a**	**d**	**g**	**h**	**Mean**	**1σ**	**G1**	**G2**	**G3**
SiO_2	41.7	39.2	41.1	41.8	41.7	41.5	41.2	1.0	42.8	41.6	41.9	42.4	45.1	45.4	43.0	44.0	1.5	47.4	48.6	48.6
TiO_2	4.1	4.5	4.1	4.1	4.3	4.1	4.2	0.2	4.0	4.1	4.2	3.6	3.7	3.7	4.3	3.8	0.3	2.8	2.9	2.8
Al_2O_3	14.7	15.4	14.5	14.6	15.0	14.5	14.8	0.3	15.3	15.7	16.1	17.0	16.7	19.6	16.9	17.6	1.4	17.5	17.5	17.8
FeO_T	9.8	12.4	10.5	9.0	9.8	11.2	10.4	1.2	10.7	11.1	11.8	11.9	10.2	9.7	11.6	10.8	1.1	10.2	10.3	10.2
MnO	0.1	0.2	0.2	0.2	0.2	0.2	0.2	0.0	0.2	0.2	0.2	0.2	0.2	0.2	0.2	0.2	0.0	0.2	0.2	0.3
MgO	6.1	5.6	5.7	6.0	5.7	6.2	5.9	0.3	5.3	5.2	5.0	4.2	3.5	3.8	4.0	3.9	0.3	2.7	2.6	2.7
CaO	13.2	10.3	12.7	13.6	13.2	13.4	12.7	1.2	12.2	11.5	11.0	10.0	11.2	8.7	10.7	10.2	1.1	6.3	6.3	6.3
Na_2O	3.6	4.1	3.7	3.5	3.6	3.8	3.7	0.2	4.4	4.7	4.8	4.6	4.7	5.3	4.5	4.8	0.4	6.2	6.2	6.3
K_2O	1.6	1.9	1.5	1.6	1.6	1.7	1.6	0.1	1.7	1.8	2.0	1.8	1.8	2.0	1.7	1.8	0.1	3.8	3.8	3.8
P_2O_5	1.1	0.9	0.9	1.0	0.9	0.9	0.9	0.1	1.0	1.0	1.1	1.2	1.4	1.4	0.8	1.2	0.3	1.3	1.2	1.1
F (ppm)	1380	1680	1740	1070	1460	1690	1572	325	2070	2200	1350	###	1860	2080	1590	2133	713	2330	2500	3000
S (ppm)	2062	2488	2187	2448	1927	2007	2166	228	325	770	465	###	1390	1085	1575	1330	244	1030	1150	990
Cl (ppm)	890	870	860	610	670	1090	875	175	840	950	1010	750	870	750	450	784	182	820	790	780
Total	96.4	95.0	95.2	95.7	96.3	97.9	95.6		97.8	97.1	98.2	97.0	98.5	99.7	97.5	98.2		98.5	99.6	99.9

	97009									97010						
Inclusion	**a**	**d**	**g**	**j**	**Mean**	**1σ**	**G1**	**G2**	**G3**	**b**	**c**	**d**	**f**	**g**	**Mean**	**1σ**
SiO_2	46.9	52.0	51.8	51.5	50.6	2.1	51.9	52.7	52.8	53.1	52.5	53.5	53.3	53.5	53.2	0.4
TiO_2	1.8	1.8	1.5	2.0	1.7	0.2	1.6	1.4	1.6	2.0	1.7	2.2	1.9	1.8	1.9	0.2
Al_2O_3	18.2	19.2	19.7	19.4	19.1	0.6	19.0	19.4	19.8	19.1	19.2	18.9	20.0	19.5	19.3	0.4
FeO_T	6.7	7.4	6.6	7.4	6.9	0.4	7.1	6.9	6.8	6.9	7.6	6.8	6.8	6.8	7.0	0.3
MnO	0.2	0.2	0.2	0.2	0.2	0.0	0.2	0.3	0.3	0.2	0.2	0.2	0.2	0.2	0.2	0.0
MgO	1.1	1.5	1.4	1.4	1.3	0.1	1.4	1.3	1.4	1.4	1.2	1.3	1.3	1.3	1.3	0.0
CaO	3.8	4.1	4.8	3.8	4.1	0.4	3.6	3.7	3.7	3.6	3.9	3.7	3.5	3.3	3.6	0.2
Na_2O	7.1	7.8	7.5	7.2	7.6	0.6	7.6	7.8	8.2	8.2	7.5	7.9	8.1	8.3	8.0	0.3
K_2O	4.9	4.9	4.7	4.9	4.9	0.2	4.9	5.1	5.0	5.0	5.2	5.1	5.3	5.3	5.2	0.1
P_2O_5	0.4	0.7	0.6	0.4	0.5	0.1	0.5	0.6	0.5	0.9	0.8	0.8	0.8	0.8	0.8	0.0
F (ppm)	1290	1410	1720	2430	1386	859	1930	1140	1590	3670	2770	2320	2230	2600	2718	574
S (ppm)	665	915	545	690	671	131	520	330	510	755	540	840	345	685	633	195
Cl (ppm)	1800	1520	1410	1610	2172	2053	1580	1480	1280	1410	1000	1420	1250	1200	1256	173
Total	91.6	99.9	99.2	98.5	98.4		98.1	99.3	100.5	101.0	100.1	100.8	101.5	101.0	101.1	

	97011						97018					
Inclusion	**a**	**b**	**c**	**f**	**Mean**	**1σ**	a	c	e	f	Mean	1σ
SiO_2	52.9	53.3	52.4	53.8	53.1	0.6	55.3	54.1	56.0	55.1	55.1	0.8
TiO_2	1.3	1.4	1.3	1.3	1.3	0.1	0.9	1.1	1.0	0.9	1.0	0.1
Al_2O_3	19.6	20.3	19.8	20.5	20.1	0.4	19.5	19.6	20.1	20.3	19.9	0.4
FeO_T	5.6	5.3	5.5	5.7	5.5	0.2	5.4	5.4	5.3	5.5	5.4	0.1
MnO	0.3	0.2	0.2	0.3	0.2	0.0	0.3	0.4	0.2	0.2	0.3	0.1
MgO	0.9	0.9	1.0	0.9	0.9	0.0	0.9	0.9	0.8	0.9	0.8	0.0
CaO	3.2	3.0	2.6	2.9	3.0	0.2	1.9	1.9	1.9	1.8	1.9	0.1
Na_2O	7.5	8.6	8.1	8.3	8.1	0.5	8.7	8.6	9.0	9.1	8.9	0.2
K_2O	5.5	5.7	5.3	5.6	5.5	0.2	5.6	5.6	5.6	5.9	5.7	0.2
P_2O_5	0.7	0.8	0.6	0.5	0.7	0.2	0.3	0.3	0.3	0.2	0.3	0.0
F (ppm)	1770	2270	2260	1470	1943	392	2250	1880	2870	1410	2103	616
S (ppm)	420	600	515	670	551	108	225	290	610	350	369	169
Cl (ppm)	1330	1370	1370	1430	1375	41	1320	1530	1630	1390	1468	139
Total	97.9	99.9	97.2	100.0	99.5		99.1	98.0	100.8	100.2	100.5	

MAGNETITE FRACTIONATION AND DIFFERENTIATION

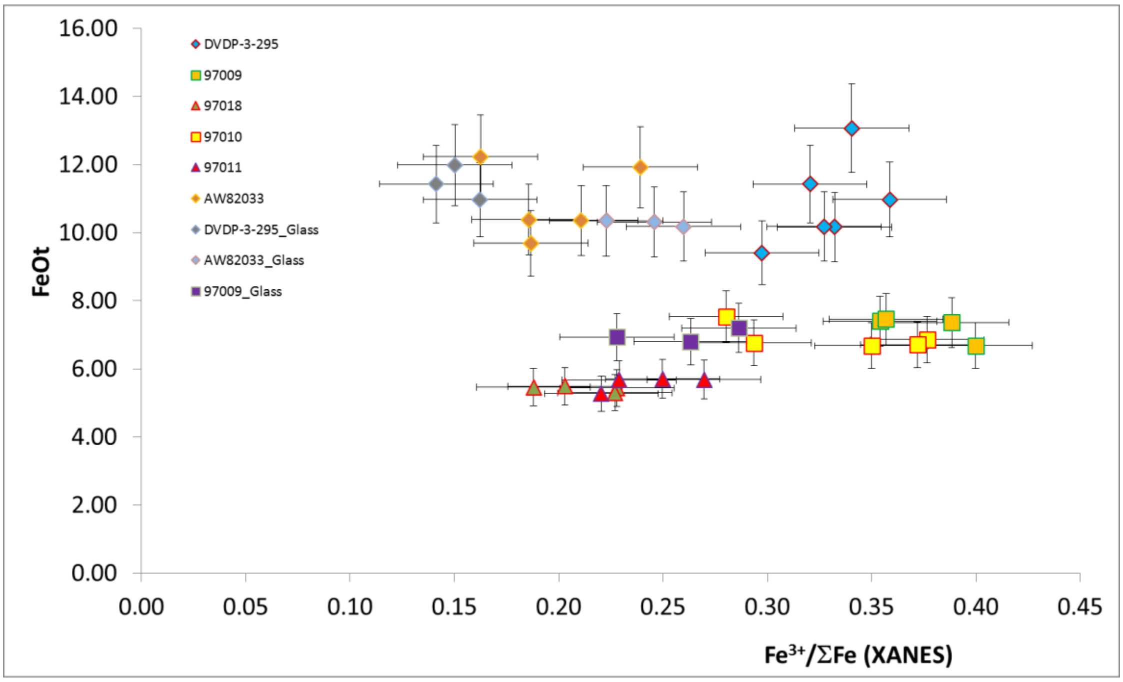

Figure S9: *Plot of $Fe^{3+}/\Sigma Fe$ ratios compared to the melt iron content (as FeOt in wt%). The absence of correlation between the iron content and the $Fe^{3+}/\Sigma Fe$ ratios shows that magnetite precipitation is unlikely to exert a strong influence on the melt redox state.*

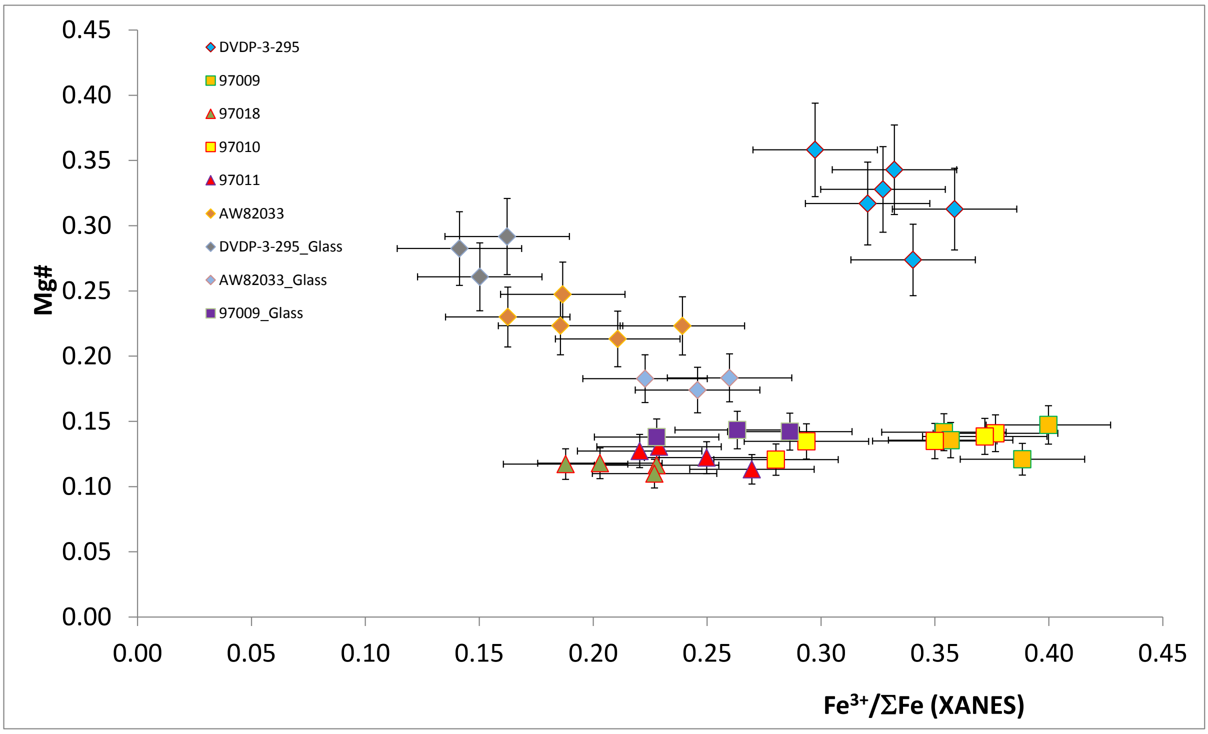

Figure S10: *Plot of $Fe^{3+}/\Sigma Fe$ ratios compared to the Mg number, defined as MgO/(MgO + FeO). The Mg number can be used as a proxy for differentiation. The absence of correlation between Mg# and the $Fe^{3+}/\Sigma Fe$ ratios shows that there is no obvious change in redox with differentiation.*

POST-ENTRAPPMENT MODIFICATIONS

There are two main processes that bear the potential to modify the composition of melt inclusions. The first one is the diffusion of element between the melt and its host crystal. Of particular importance here is the diffusion of Fe from the melt to the host mineral in the case of olivine-hosted MI (e.g.Danyushevsky *et al.*, (2000)). The second, possibly more important, process is the post-entrapment crystallization of the host on the MI rim. While post-entrapment crystallization in anorthoclase-hosted MI should have little effect on the melt $Fe^{3+}/\Sigma Fe$ ratio, the equivalent for olivine hosted MI would result in oxidation of both Fe and S species in the MI. Considering the complexity in modeling post-entrapment crystallization (PEC), the lack of consensus among authorities in the field and the fact that uncertainty in the calculated PEC will result in large uncertainty in the re-calculated MI $Fe^{3+}/\Sigma Fe$ and $S^{6+}/\Sigma S$ ratios we chose not to attempt any correction. Nevertheless we report in table S6 the composition of the host olivine mineral (from Eschenbacher, (1998)) together with estimates of the amount of post-entrapment crystallization (PEC in %), which ranges from 0 to 4.2% and calculated using the *petrolog3* freeware (Danyushevsky and Plechov, 2011). Calculation of PEC were conducted using the Fe^{3+}/Fe^{2+} measurement from XANES analyses for each MI. Figure S11 shows that there is no correlation between the calculated amount of PEC and the $Fe^{3+}/\sum Fe$ ratio of the MI, hence demonstrating that the observed redox trend cannot be a reflection of differences in the amount of PEC.

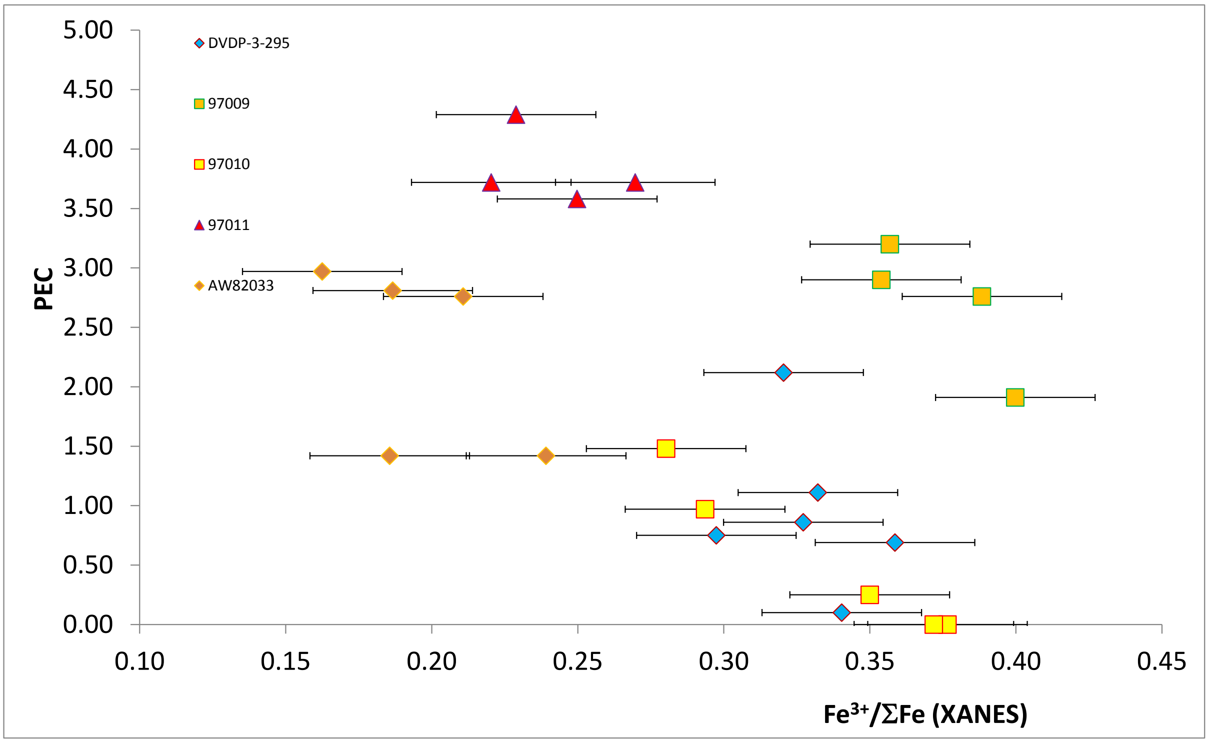

Figure S11: *Plot of $Fe^{3+}/\Sigma Fe$ ratio determined by Fe K-edge XANES compared to calculated amount of post-entrapment crystallization (in %) for each melt inclusion. Calculated negative values of PEC are reported as zero. Errors in calculated PEC are unconstrained; errors in $Fe^{3+}/\Sigma Fe$ ratios are discussed bellow.*

Table S6. Olivine host compositions from Eschenbacher, (1998) and Oppenheimer *et al.*, (2011) *and post-entrapment crystallisation estimate (PEC)*

DVDP-3-295

Host	b	c	g	j	q	r	Mean	1σ
SiO2	39.1	38.5	38.5	40.3	40.0	38.8	39.2	0.8
FeO	13.1	18.3	14.8	13.2	14.1	13.3	14.4	2.0
MnO	0.2	0.3	0.2	0.2	0.3	0.2	0.2	0.0
MgO	46.5	42.0	45.2	46.0	45.3	45.9	45.2	1.6
CaO	0.3	0.3	0.3	0.3	0.3	0.4	0.3	0.0
Total	99.1	99.3	99.1	100.0	100.1	98.6	99.4	0.6
Fa	13.6	19.6	15.5	13.9	14.9	14.0	15.2	2.2
Fo	86.4	80.4	84.5	86.1	85.1	86.0	84.8	2.2
FeT/Mg	0.16	0.24	0.18	0.16	0.17	0.16	0.18	
Mg#	0.86	0.80	0.85	0.86	0.85	0.86	0.85	
Kd*	0.08	0.09	0.08	0.09	0.09	0.08	0.08	
PEC**	1.11	0.10	0.69	0.75	0.86	2.12	0.94	

AW82033

Host	a	c	d	g	h	Mean	1σ
SiO2	38.8	38.2	38.4	38.9	37.2	38.3	0.7
FeO	22.1	20.5	23.4	19.6	22.8	21.7	1.6
MnO	0.3	0.3	0.3	0.2	0.4	0.3	0.1
MgO	40.0	39.4	38.8	42.6	39.7	40.1	1.5
CaO	0.3	0.3	0.4	0.4	0.4	0.3	0.0
Total	101.4	98.6	101.2	101.5	100.5	100.7	1.2
Fa	23.6	22.6	25.3	20.5	24.4	23.3	1.8
Fo	76.4	77.4	74.7	79.5	75.6	76.7	1.8
FeT/Mg	0.31	0.29	0.34	0.26	0.32	0.30	
Mg#	0.76	0.77	0.75	0.79	0.76	0.77	
Kd*	0.09	0.08	0.10	0.08	0.09	0.09	
PEC**	2.97	2.76	1.42	2.81	1.42	2.28	

97009

Host	a	d	g	j	Mean	1σ
SiO2	30.8	35.7	36.0	34.7	34.3	2.4
FeO	34.1	34.5	32.0	34.2	33.7	1.1
MnO	0.8	1.0	0.8	1.0	0.9	0.1
MgO	26.0	29.1	31.0	28.3	28.6	2.1
CaO	0.4	0.5	0.4	0.4	0.4	0.0
Total	92.1	100.8	100.3	98.5	97.9	4.0
Fa	27.0	25.5	24.2	25.7	25.6	1.1
Fo	73.0	74.5	75.8	74.3	74.4	1.1
FeT/Mg	0.74	0.67	0.58	0.68	0.66	
Mg#	0.58	0.60	0.63	0.60	0.60	
Kd*	0.10	0.11	0.10	0.11	0.11	
PEC**	2.76	2.90	1.91	3.20	2.69	

97010

Host	b	c	d	f	g	Mean	1σ
SiO2	36.8	35.7	36.3	36.1	36.6	36.3	0.5
FeO	31.3	33.2	31.3	32.1	31.6	31.9	0.8
MnO	1.1	1.1	1.0	1.0	1.0	1.0	0.1
MgO	31.5	29.0	31.6	30.8	31.8	30.9	1.1
CaO	0.4	0.4	0.4	0.4	0.4	0.4	0.0
Total	101.2	99.4	100.5	100.3	101.3	100.5	0.8
Fa	35.8	39.1	35.7	36.9	35.8	36.7	1.5
Fo	64.2	60.9	64.3	63.1	64.2	63.3	1.5
FeT/Mg	0.56	0.64	0.55	0.58	0.56	0.58	
Mg#	0.64	0.61	0.64	0.63	0.64	0.63	
Kd*	0.09	0.09	0.09	0.09	0.09	0.09	
PEC*	<0	1.48	0.97	<0	0.25	0.90	

97011

Host	a	b	c	f	Mean	1σ
SiO2	33.8	35.7	35.8	35.9	35.3	1.0
FeO	33.3	33.3	30.0	33.7	32.6	1.7
MnO	1.2	1.1	1.0	1.2	1.1	0.1
MgO	28.1	29.6	29.9	29.1	29.2	0.8
CaO	0.4	0.4	0.4	0.4	0.4	0.0
Total	96.7	100.2	97.1	100.2	98.5	1.9
Fa	25.6	25.0	23.6	25.2	24.8	0.9
Fo	74.4	75.0	76.4	74.8	75.2	0.9
FeT/Mg	0.66	0.63	0.56	0.65	0.63	
Mg#	0.60	0.61	0.64	0.61	0.61	
Kd*	0.09	0.09	0.08	0.08	0.09	
PEC*	3.58	3.72	4.29	3.72	3.83	

* *Partition coefficient (Kd) for the Fe/Mg ratio between the olivine and MI it host. **PEC calculated using petrolog3* (Danyushevsky and Plechov, 2011))

ERROR ANALYSIS

Error on the centroid position for each MI spectra has been fully attributed to the error in the determination of spectra shift correcting for instrumental energy drift. The error associated to this shift has been determined to be 0.03eV as this value represents the maximum difference in energy shift between spectra from similar compositions relative to their reference spectra. The error in determining the centroid by pre-edge region fitting is dwarfed in comparison. Error on the calibration line (fitted by the least-squares method) relating the centroid position relative to $Fe^{3+}/\Sigma Fe$ was determined using the following standard formulas:

$$Slope\ error = \delta_a = \sqrt{\frac{\sum(y_i - ax_i - b)^2}{n-2}} \times \sqrt{\frac{n}{(n\sum x_i^2) - (\sum x_i)^2}}$$

$$Intercept\ error = \delta_b = \sqrt{\frac{\sum(y_i - ax_i - b)^2}{n-2}} \times \sqrt{\frac{\sum x_i^2}{(n\sum x_i^2) - (\sum x_i)^2}}$$

Where *a* is the slope and *b* the intercept. These formulas assume that each y_i point in the calibration has the same error which in our case is correct. The final error on the $Fe^{3+}/\Sigma Fe$, following standard methods becomes:

$$\delta_x = |x|\sqrt{\left(\frac{\delta_y + \delta_b}{y - b}\right)^2 + \left(\frac{\delta_a}{a}\right)^2}$$

With *x* the $Fe^{3+}/\Sigma Fe$ ratio and *y* the centroid position in eV. It is to be noted that about 40 to 60% of the final error on the $Fe^{3+}/\Sigma Fe$ ratio is due to the error on the calibration, which is a systematic error. The error associated with measurement uncertainty can be expressed as:

$$\delta_x = \left|\frac{1}{a}\right| \times \delta_y$$

It is this last error that is reported on all figures.

REFERENCES

1. Eschenbacher, A. (1998). Open-system degassing of a fractionating, alkaline magma, Mount Erebus, Ross Island, Antarctica.
2. Oppenheimer, C. *et al.* (2011). Mantle to surface degassing of alkalic magmas at Erebus volcano, Antarctica. *Earth Planet. Sci. Lett.* **306**, 261–271
3. Danyushevsky, L. V., Della-Pasqua, F. N. & Sokolov, S. (2000). Re-equilibration of melt inclusions trapped by magnesian olivine phenocrysts from subduction-related magmas: petrological implications. *Contrib Mineral Petrol* **138**, 68–83
4. Danyushevsky, L. V. & Plechov, P. (2011). Petrolog3: Integrated software for modeling crystallization processes. *Geochemistry, Geophysics, Geosystems* **12**, n/a–n/a